Progress In Electromagnetics Research, *PIER 31, 55–67, 2001*

RESONANT BEHAVIOURS OF MICROSTRIP ANTENNA IN MULTILAYERED MEDIA: AN EFFICIENT FULL-WAVE ANALYSIS

L. Xia, C.-F. Wang, L.-W. Li, P.-S. Kooi, and M.-S. Leong

Department of Electrical and Computer Engineering
The National University of Singapore
10 Kent Ridge Crescent, Singapore 119260

Abstract–This paper presents an efficient analysis of a microstrip antenna in multilayered media using the method of moments (MoM). The general forms of spectral-domain Green's functions for multilayered media are converted into the spatial-domain Green's functions using the discrete complex image method (DCIM). With the spatial-domain Green's functions, the mixed potential integral equation (MPIE) is discretized in spatial domain, and the resultant system of equations is then solved using the biconjugate gradient (BCG) method. As applications, resonant frequencies of microstrip antennas in multilayered media are analysed. The numerical results show that the present method is an efficient and accurate scheme for analysing microstrip antennas in multilayered media.

1. INTRODUCTION

Simulating the behavior of microstrip structure in multilayered media is very important for the design of microstrip antennas and monolithic microwave integrated circuits (MMIC's). There are many approaches that can be applied to achieve this objective. Generally speaking, simulation methods can be broadly divided into two kinds. Finite

element method (FEM) [1] and finite-difference time-domain (FDTD) [2] method fall into the first kind for solving differential equations. Method of moments (MoM) [3] falls into the second kind for solving integral equations. Among them, the MoM based on integral equations is robust and has several advantages over FEM or FDTD method. First, the solution from the MoM is found using the 2-D surface of perfect electric conductor (PEC), while the solution from either FEM or FDTD is solved for from the 3-D space, so the number of unknowns in FEM or FDTD is substantially lager than that in integral equation method. Under circumstances involving small objects with relatively large distances among them, the MoM is much more efficient or faster than the other two. Second, the MoM has no absorbing boundary condition (ABC) issue which can lead to unstable solutions when the ABC is used in FDTD and FEM to reduce an open-system to a finite region problem.

Both electric field integral equation (EFIE) and mixed potential integral equation (MPIE) [4] can be used for MoM. It is reported that MoM based on MPIE is more efficient for antenna problem in multilayered media, because MPIE provides a less possibly singular kernel compared with EFIE.

In order to solve MPIE in multilayered media using the spatial domain MoM, the spatial-domain Green's functions for multilayered media have to be calculated first from its spectral domain counterparts [5], in which Sommerfeld integral (SI) will occur and no analytical solution is available. The SI can be solved either in numerical integration which is very time consuming or using other approximated methods. In this paper, the discrete complex image method (DCIM) [6–9] is adopted. Generally speaking, the DCIM is to approximate the spectral kernel by a sum of complex exponentials using the Prony method or the generalized pencil-of-function (GPOF) technique. Then, the SI could be evaluated in close form via the Sommerfeld identity. With the spatial domain Green's functions, the MPIE is then discretized in spatial domain, and the resultant system of equations is solved using the biconjugate gradient (BCG) method [10–13]. As an application, microstrip antennas of arbitrary shapes in multilayered media are analysed in this paper. The numerical results show that the present method is an efficient and accurate method for analysing the microstrip structure in multilayered media and can be further extended to the analysis and design of MMIC's.

2. FORMULATIONS

The boundary condition on a perfectly conducting surface is that the tangential electric field on the conductor equals to zero. That is,

$$\hat{n} \times \mathbf{E}^s(\mathbf{r}) = -\hat{n} \times \left[\mathbf{E}^i(\mathbf{r}) + \mathbf{E}^r(\mathbf{r})\right], \qquad \text{on } S; \tag{1}$$

where S is the conducting surface, $\mathbf{E^s}$ denotes the scattered field excited by the current on S, $\mathbf{E^i}$ stands for the incident electric field, and $\mathbf{E^r}$ identifies the reflected field by the dielectric substrate in the absence of patch. The $\mathbf{E^i}$ and $\mathbf{E^r}$ can be expressed respectively as

$$\begin{cases} \mathbf{E}^i(\mathbf{r}) = \left(\hat{\theta}^i E_\theta + \hat{\phi}^i E_\phi\right) e^{-j\mathbf{k}^i \cdot \mathbf{r}} \\ \mathbf{E}^r(\mathbf{r}) = \left(\hat{\theta}^r R^{TM} E_\theta + \hat{\phi}^r R^{TE} E_\phi\right) e^{-j\mathbf{k}^r \cdot \mathbf{r}} \end{cases} \tag{2}$$

where R^{TM} and R^{TE} are the general reflection coefficients at the interface of the patch for the TE and TM incidences, respectively. The MPIE for (1) can be written as

$$j\omega\mu_0 \hat{n} \times \left[\mathbf{A}(\mathbf{r}) + \frac{1}{k_0^2}\nabla\Phi(\mathbf{r})\right] = \hat{n} \times \left[\mathbf{E}^i(\mathbf{r}) + \mathbf{E}^r(\mathbf{r})\right] \tag{3}$$

with

$$\begin{cases} \mathbf{A}(\mathbf{r}) = \displaystyle\iint_S \overline{\mathbf{G}}_A(\mathbf{r}, \mathbf{r}') \cdot \mathbf{J}(\mathbf{r}') ds', \\ \Phi(\mathbf{r}) = \displaystyle\iint_S G_q(\mathbf{r}, \mathbf{r}') \nabla \cdot \mathbf{J}(\mathbf{r}') ds'; \end{cases} \tag{4}$$

in which $\mathbf{J}(\mathbf{r})$ is the unknown current on the patch, and $\overline{\mathbf{G}}_A$ and G_q are spatial domain Green's functions for the magnetic vector potential and the electric scalar potential, respectively.

To solve the integral equation (3) by the MoM, the patch is first divided into small mesh rectangles, and then the current on the patch is expanded with rooftop basis functions,

$$\mathbf{J}(\mathbf{r}) = \sum_{m,n} I^x_{m,n} \mathbf{f}^x_{m,n} + \sum_{m,n} I^y_{m,n} \mathbf{f}^y_{m,n} \tag{5}$$

where $\mathbf{f}^x_{m,n} = f^x_{m,m}\hat{x}$ and $\mathbf{f}^y_{m,n} = f^y_{m,m}\hat{y}$ are vector rooftop basis functions in the x and y directions. Applying the Galerkin's method to the equation (3), we can get the following matrix equation

$$\begin{bmatrix} \mathbf{G}_{xx} & \mathbf{G}_{xy} \\ \mathbf{G}_{yx} & \mathbf{G}_{yy} \end{bmatrix} \begin{bmatrix} \mathbf{J}_x \\ \mathbf{J}_y \end{bmatrix} = \begin{bmatrix} \mathbf{b}_x \\ \mathbf{b}_y \end{bmatrix} \tag{6}$$

where

$$\begin{aligned}
\mathbf{G}_{xx} &= \left[G_{xx}(m-m', n-n')\right], \\
\mathbf{G}_{xy} &= \left[G_{xy}(m-m', n-n')\right], \\
\mathbf{G}_{yx} &= \left[G_{yx}(m-m', n-n')\right], \\
\mathbf{G}_{yy} &= \left[G_{yy}(m-m', n-n')\right], \\
\mathbf{b}_x &= \left[\left\langle \mathbf{f}^x_{m,n}, \mathbf{E}^i(\mathbf{r}) + \mathbf{E}^r(\mathbf{r})\right\rangle\right], \\
\mathbf{b}_y &= \left[\left\langle \mathbf{f}^y_{m,n}, \mathbf{E}^i(\mathbf{r}) + \mathbf{E}^r(\mathbf{r})\right\rangle\right];
\end{aligned}$$

with

$$\begin{aligned}
G_{xx}(m-m', n-n') &= \Gamma^x_a(m-m', n-n') + \Gamma_{xx}(m-m', n-n'), \\
G_{xy}(m-m', n-n') &= \frac{1}{\Delta x \Delta y} \sum_{i=0}^{1} \sum_{k=0}^{-1} (-1)^{i+k} \Gamma_q(m-m'+i, n-n'+k), \\
G_{yy}(m-m', n-n') &= \Gamma^y_a(m-m', n-n') + \Gamma_{yy}(m-m', n-n'), \\
G_{yx}(m-m', n-n') &= G_{xy}(n'-n, m'-m),
\end{aligned}$$

and

$$\begin{aligned}
\Gamma_{xx}(m-m', n-n') &= \frac{1}{(\Delta x)^2} \sum_{i=0}^{1} \sum_{k=0}^{-1} (-1)^{i+k} \Gamma_q(m-m'+i+k, n-n'), \\
\Gamma_{yy}(m-m', n-n') &= \frac{1}{(\Delta y)^2} \sum_{i=0}^{1} \sum_{k=0}^{-1} (-1)^{i+k} \Gamma_q(m-m', n-n'+i+k), \\
\Gamma^x_a(m-m', n-n') &= j\omega\mu_0 \iint_S f^x_{m,n} \iint_S G_a f^x_{m',n'} ds' ds, \\
\Gamma^y_a(m-m', n-n') &= j\omega\mu_0 \iint_S f^y_{m,n} \iint_S G_a f^y_{m',n'} ds' ds, \\
\Gamma_q(m-m', n-n') &= \frac{j}{\varpi\varepsilon_0} \iint_S \Pi_{m,n} \iint_S G_q \Pi_{m',n'} ds' ds.
\end{aligned}$$

In the above, G_a denotes the xx or yy component of $\overline{\mathbf{G}}_A$, and $\Pi_{m,n}$ is the two-dimensional unit pulse function defined over (m,n)th rectangular cell. The current distribution on microstrip antenna can then be obtained by solving the matrix equation (6) using BCG [10–13]. The resonant frequency for the microstrip antenna is the frequency at which the imaginary part of current is zero.

For the method above-mentioned, the spatial domain Green's functions G_a and G_q are the critical points to the realization of MPIE in the spatial domain. It is required to convert the spectral domain Green's function into the spatial domain one. Using the method described by [5], the close form spectral-domain Green's function (field point is in the layer n) for a horizontal electric dipole (HED) which is located in layer m (as show in Fig. 1) could be achieved after the following procedure:

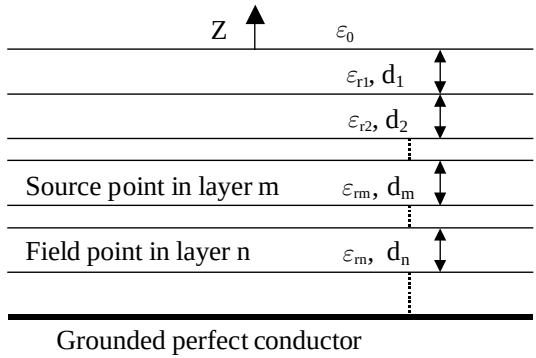

Figure 1. Multilayered medium structure.

$$\tilde{G}_a = \frac{\mu_m}{2jk_{mz}} F_n^{TE}, \tag{7}$$

$$\tilde{G}_q = \frac{1}{2j\varepsilon_n k_{mz} k_\rho^2} \left(\frac{\mu_m k_n^2}{\mu_n} F_n^{TE} - jk_{mz} \frac{\partial}{\partial z} F_n^{TM} \right), \tag{8}$$

where F_n^{TE} and F_n^{TM} can be expressed respectively depending on the following 3 different situations: $m = n$, $m > n$, and $m < n$, and the explicit expressions are suppressed here. The spatial domain Green's functions can be obtained from their spectral domain counterparts through inverse Hankel function transform as follows:

$$G_{a,q}(\rho) = \frac{1}{4\pi} \int_{-\infty}^{+\infty} \tilde{G}_{a,q}(k_\rho) H_0^{(2)}(k_\rho \rho) k_\rho dk_\rho \tag{9}$$

where the $H_0^{(2)}$ identified the Hankel function of the second kind. By using the discrete complex image method as developed in [6, 7], the inverse transform of the quasi-static contribution is evaluated using

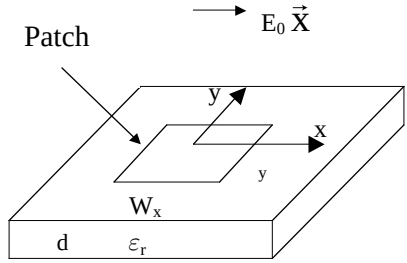

Figure 2. A microstrip antenna in a single-layered structure.

the Sommerfeld identity. After extracting the quasi-static contribution, which can be done by assuming the frequency is equal to zero or $k_\rho \to \infty$, the remained can be approximated by a sum of complex exponentials, and their contribution to spatial domain Green's functions can be achieved using the Sommerfeld identity again. The spatial domain Green's functions can be written as follows

$$\begin{cases} G_{a,q} = G_{a,q}^{(qd)} + G_{a,q}^{(ci)}, \\ G_{a,q}^{(ci)} = \sum_{i=1}^{N_c} a_i \dfrac{e^{-jk_0 r_i}}{4\pi r_i}, \end{cases} \tag{10}$$

where $r_i = \sqrt{\rho^2 - b_i^2}$ is complex, $G_{a,q}^{(qd)}$ represents the quasi-static contributions, N_c denotes the number of complex images, and the coefficients a_i and b_i are determined by the generalized pencil-of-function (GPOF) method. As mentioned in [8] and [14], when source is in the bounded region of multilayered media, the modification of DCIM is necessary. In this case, the exponentials are written in terms of the propagation constant of the unbounded layer instead of that of the source layer.

3. RESULTS AND DISCUSSION

In this section, we present some numerical results to demonstrate the accuracy and efficiency of the method described above. The first example concerns the current distribution over a square patch antenna in a single-layered structure as in Fig. 2 at x-polarized plane wave excitation. The calculated current distribution is shown in Fig. 3 and compared with that from Bailey et al. [15]. The two sets of results

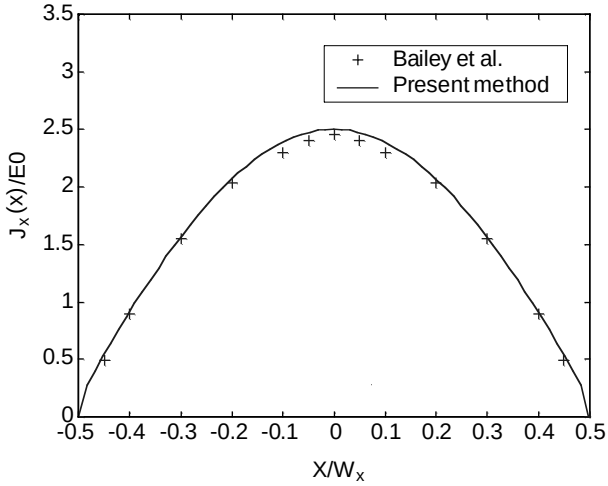

(a) A function of x at $y = 0$

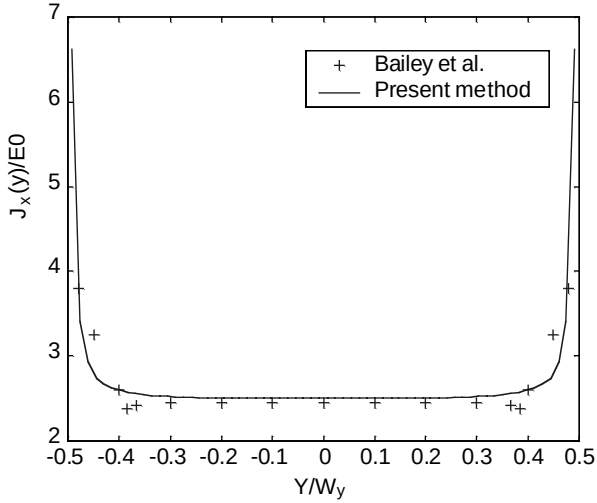

(b) A function of y at $x = 0$

Figure 3. X-directed current distribution of a patch antenna ($W_x = W_y = 0.48\,\lambda_e$, $d = 0.02\,\lambda_e$, and $\varepsilon_r = 2.5$, where λ_e is the wavelength in dielectric).

agree very well. Table 1 also shows the calculated resonant frequencies for some single-layered structures and the experimental data [16] are also included for comparison. We can see that they agree quite well.

Table 1. Calculated and experimental resonant frequencies for single layer microstrip antenna.

ε_r	W_x (cm)	W_y (cm)	d (cm)	Experimental [16] f_r	Calculated f_r
2.24	3.3	12	0.051	3.03 GHz	2.97 GHz
2.24	3.25	12	0.079	3.02 GHz	3.00 GHz
2.24	3.15	12	0.157	3.02 GHz	3.00 GHz
2.24	3.9	14.4	0.079	2.51 GHz	2.51 GHz
2.24	2.7	10.3	0.079	3.53 GHz	3.59 GHz

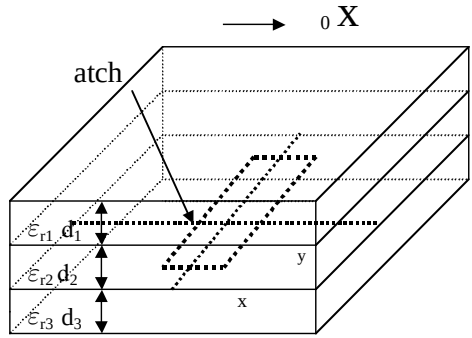

Figure 4. A microstrip antenna in a multilayered structure.

The second example demonstrates the resonant frequency shift of the dielectric-covered microstrip antennas (microstrip antenna in a multilayered structure as shown in Fig. 4) compared with uncovered ones. First we analysed some particular structures and compared the results with experimental data [17], and results are listed in Table 2. From Table 2, we can see that the resonant frequency of the microstrip antenna with a dielectric superstrate becomes smaller than that without the dielectric superstrate and the calculated ones agree well with the experimental ones. Then we consider the effect of dielectric superstrate for different patch dimension. The results are shown in Fig. 5, and Fig. 5 reveals that when the patch becomes larger and larger, the difference between the resonant frequencies in the presence and absence of superstrate becomes less notable. This is because the relative configuration variance brought by its dielectric superstrater is less significant when the patch grows larger.

The third example considered resonant behaviours of the rectangular patch antenna in a three layered structure excited by an x-polarized

Table 2. Calculated and experimental data for the resonant frequencies of a microstrip antenna in the case of different superstrates: $\varepsilon_{r2} = 2.32$, $d_2 = 1.59\,\text{mm}$, $W_x = 22.9\,\text{mm}$, and $W_y = 19.0\,\text{mm}$.

Dielectric Cover	ε_{r1}	d_1 (mm)	f_r (GHz) Experimental [17]	f_r (GHz) Calculated	$\Delta f_r/f_r$ (%) Experimental [17]	$\Delta f_r/f_r$ (%) Calculated
Air	1.0	-	4.104	4.072	0	0
Duroid	2.32	0.8	4.008	3.964	2.34	2.65
		1.59	3.934	3.916	4.14	3.83
		3.18	3.895	3.862	5.09	5.16
Plexiglass	2.6	1.12	3.952	3.917	3.70	3.81
		1.59	3.912	3.887	4.68	4.54
		3.18	3.874	3.823	5.60	6.11
		6.36	3.806	3.763	7.26	7.59

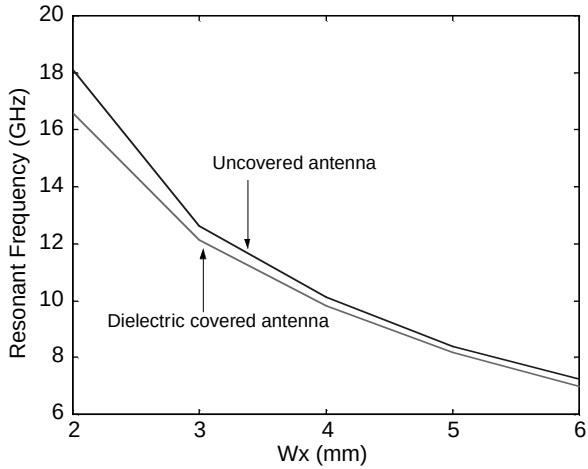

Figure 5. Resonant frequency shift of a microstrip antenna as a function of patch dimension in the presence and absence of a superstrate ($W_x = W_y$, $\varepsilon_{r1} = 20$, $d_1 = 0.0127\,\text{mm}$, $\varepsilon_{r2} = 10.2$, $d_2 = 1.27\,\text{mm}$, and the patch is mounted on the interface between dielectrics 1 and 2).

plane wave. The resonant behaviours are shown in Fig. 6. For comparison, we also include the resonant behaviour in the absence of superstrates. From Fig. 6, we can see that the resonant frequency for the three-layered structure is 9.05 GHz, and the resonant frequency in the absence of superstrates is 9.18 GHz. The shift is about 1.41of superstrates, respectively, and the shift is about 1.75%.

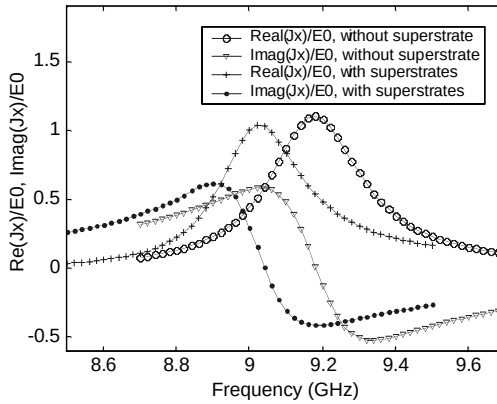

Figure 6. Resonant behaviour of a rectangular patch antenna in the three-layered structure and single-layered structure excited by plane wave. For the three-layered structure, $\varepsilon_{r1} = 10.5$, $d_1 = 3.302\,\text{mm}$, $\varepsilon_{r2} = 1.006$, $d_2 = 14.81\,\text{mm}, \varepsilon_{r3} = 2.17$, $d_3 = 0.508\,\text{mm}$, $W_x = 10.444\,\text{mm}, W_y = 15.666\,\text{mm}$, and the patch is mounted on the interface between dielectrics 2 and 3. For single-layered structure, $\varepsilon_r = 2.17$, $d = 0.508\,\text{mm}$, $W_x = 10.444\,\text{mm}, W_y = 15.666\,\text{mm}$, and the patch is mounted on the interface of dielectric and air.

As the fourth example, we consider the shift of resonant frequency as a function of thickness and dielectric constant of the superstrate used for microstrip antennas in two- and three- layered structures. For the two-layered structure, the structure parameters and results are shown in Fig. 7 and Table 3, and the structure parameters and results for the three-layered structure can be found in Fig. 8 and Table 4. From the Fig. 7 and 8, we can see that if the thickness of the top superstrate becomes unlimited small, the resonant frequency will equal to that of the structure without this layer, and this is also what we can conclude from physical concept.

Table 3. Resonant frequencies of a microstrip antenna versus ε_{r1} for a two-layered structure: $\varepsilon_{r2} = 2.17$, $d_1 = 0.63\,\text{mm}$, $d_2 = 0.508\,\text{mm}$, $W_x = 10.444\,\text{mm}$, and $W_y = 10.444\,\text{mm}$. The patch is mounted on the interface between dielectrics 1 and 2.

ε_{r1}	1.0	2.17	2.33	2.50	2.55	10.2	10.5
Resonant Frequency (GHz)	9.28	9.06	9.02	8.99	8.98	8.00	7.97

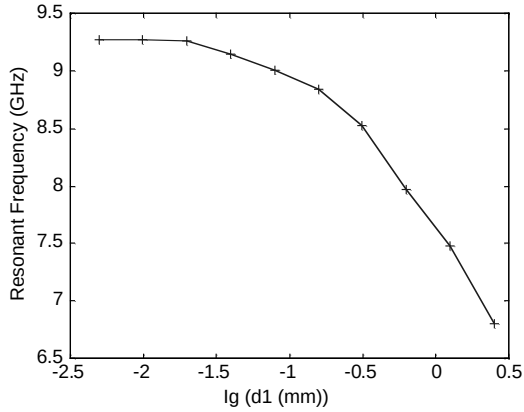

Figure 7. Resonant frequency of a microstrip antenna in a two-layered structure versus the superstrate thickness ($\varepsilon_{r1} = 10.5$, $\varepsilon_{r2} = 2.17$, $d_2 = 0.508\,\text{mm}$, d_1 changes from $\lambda_1/2^2$ to $\lambda_1/2^{11}$, λ_1 is the wavelength in dielectric 1 at the resonant frequency (9.28 GHz) in the absence of the superstrate. $W_x = 10.444\,\text{mm}$, $W_y = 10.444\,\text{mm}$, and the patch is mounted on the interface between dielectrics 1 and 2).

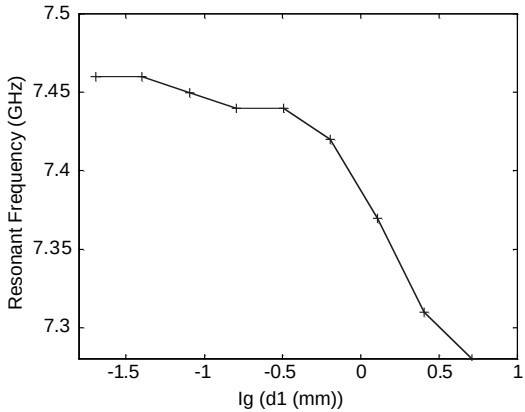

Figure 8. Resonant frequency of a microstrip antenna in a three-layered structure versus the superstrate thickness ($\varepsilon_{r1} = 2.55$, $\varepsilon_{r2} = 10.5$, $\varepsilon_{r3} = 2.17$, $d_2 = 1.26\,\text{mm}$, $d_3 = 0.508\,\text{mm}$, d_1 changes from $\lambda_1/2^2$ to $\lambda_1/2^{10}$, λ_1 is the wavelength in dielectric 1 at the resonant frequency (9.28 GHz) in the absence of superstrates. $W_x = 10.444\,\text{mm}$, $W_y = 10.444\,\text{mm}$, and the patch is mounted on the interface between dielectrics 2 and 3). The resonant frequency is 7.48 GHz in the absence of top superstrate.

Table 4. Resonant frequencies of a microstrip antenna versus ε_{r1} for a three-layered structure: $\varepsilon_{r2} = 10.5$, $\varepsilon_{r3} = 2.17$, $d_1 = 1.28\,\text{mm}$, $d_2 = 1.26\,\text{mm}$, $d_3 = 0.508\,\text{mm}$, $W_x = 10.444\,\text{mm}$, and $W_y = 10.444\,\text{mm}$. The patch is flush-mounted on the interface between dielectrics 2 and 3.

ε_{r1}	1.0	2.17	2.33	2.50	2.55	10.2	10.5
Resonant Frequency (GHz)	7.48	7.40	7.40	7.38	7.38	6.82	6.80

4. CONCLUSION

In this article, the MoM is applied to characterize microstrip antennas in multilayered media by solving MPIE. Several numerical results are obtained and it is demonstrated that the present method is an efficient and accurate one for modelling microstrip structures of multilayers. This is especially useful for designing MMIC passive components in multilayered media.

REFERENCES

1. Jin, J. M., *The Finite Element Method in Electromagnetics,* Wiley, New York, 1993.
2. Taflove, A., *Computional Electromagentics: The Finite-Difference Time-Domain Method,* Artech House, Norwood, MA, 1995.
3. Harrington, R. F., *Field Computation in Electromagnetics,* Wiley, New York, 1993.
4. Mosig, J. R., "Arbitrarily shaped microstrip structures and their analysis with a mixed potential integral equation," *IEEE Trans. Microwave Theory Tech.,* Vol. MTT-36, 314–323, Feb. 1988.
5. Chew, W. C., *Waves and Fields in Inhomogeneous Media,* Van Nostrand, New York, 1990.
6. Fang, D. G., J. J. Yang, and G. Y. Delisle, "Discrete image theory for horizontal electric dipoles in a multilayered medium above a conducting ground plane," *Proc. Inst. Elec. Eng.,* Vol. 135, 297–303, 1988.
7. Chow, Y. L., J. J. Yang, D. G. Fang, and G. Y. Delisle, "A Close-form spatial Green's function for the thick microstrip substrate," *IEEE Trans. Microwave Theory Tech.,* Vol. MTT-39, 588–592, Mar. 1991.
8. Kipp, R. A. and C. H. Chan, "Complex image method for sources in bounded region of multiplayer," *IEEE Trans. Microwave Theory Tech.,* Vol. MTT-42, 860–865, May 1994.

9. Akson, M. I., "A robust approach for the derivation of closed-form Green's function," *IEEE Trans. Microwave Theory Tech.,* Vol. MTT-44, 651–658, May 1996.
10. Jin, J. M. and J. L. Volakis, "A biconjugate gradient solution for scattering by plane plates," *Electromagn.,* Vol. 12, 105–119, 1992.
11. Lanczos, C., "An iteration method for the solution of the eigenvalue problem of linear differential and integral operators," *J. Res. Nat. Bur. Stand.,* Vol. 45, 255–282, 1950.
12. Smith, C. F., A. F. Peterson, and R. Mittra, "The biconjugate gradient method for electromagnetic scattering," *IEEE Trans. Antennas Propagat.,* Vol. AP-38, 1530–1536, Oct. 1990.
13. Wang, C. F., F. Ling, and J. M. Jin, "A fast full-wave analysis of scattering and radiation from large finite arrays of microstrip antennas," *IEEE Trans. Antennas Propagat.,* Vol. AP-46, 1467–1474, Oct. 1998.
14. Ling, F., D. Jiao, and J. M. Jing, "Efficient electromagnetic modelling of microstrip structures in multilayer media," *IEEE Trans. Microwave Theory Tech.,* Vol. MTT-47, 1810–1818, Sept. 1999.
15. Bailey, M. C. and M. D. Deshpande, "Integral equation formulation of microstrip antenna," *IEEE Trans. Antennas Propagat.,* Vol. AP-30, 651–656, July 1982.
16. Vandensande, J., H. Pues, and A. Van de Capelle, "Calculation of the bandwidth of microstrip resonator antennas," *Proceedings of European Microwave Conference,* 116–119, 1979.
17. Bahl, I. J., P. Bhartia, and S. S. Stuchly, "Design of microstrip antennas covered with a dielectric layer," *IEEE Trans. Antennas Propagat.,* Vol. AP-30, 314–318, Mar. 1982.
18. Shen, X. H., G. A. E. Vandenbosch, and A. R. V. D. Capelle, "Study of gain enhancement method for Microstrip antenna using moment method," *IEEE Trans. Antennas Propagat.,* Vol. AP-43, 227–231, Mar. 1995.